

H.J. Karwowski, S.E. Vigdor, W.W. Jacobs, S. Kailas, P  
P.P. Singh, F.Soga and W. Ploughe\*

X rays are emitted following compound-nucleus formation as a result of internal conversion during the  $\gamma$ -cascades de-exciting evaporation residues.<sup>1)</sup> Measurements by Deconninck and Longr e<sup>2)</sup> of singles X-ray yields accompanying ( $\alpha,\text{xn}$ ) reactions suggested that if the residues are populated at sufficiently high spin, there may be a cumulative probability of emitting, on the average, significantly more than one K X-ray per residual nucleus produced. Multiple K X-ray emission is possible because the lifetime of a vacancy in the atomic K shell for heavy nuclei ( $\sim 10^{-17}$  sec) is much shorter than typical nuclear transition lifetimes. We have made the first direct measurements of K X-ray multiplicities

following fusion reactions, and we are presently studying both the nuclear structure implications of our results and the application of those results to the determination of absolute ( ${}^6\text{Li},\text{xn}$ ) cross sections.

To date, we have measured the mean K X-ray multiplicity  $\langle M_K \rangle$  for ( ${}^6\text{Li},\text{xn}$ ) reactions induced on  ${}^{181}\text{Ta}$ ,  ${}^{194,198}\text{Pt}$ ,  ${}^{197}\text{Au}$  and  ${}^{208}\text{Pb}$  at bombarding energies of 75, 85, and 95 MeV. Most of the measurements have been made via detection of X-ray-X-ray coincidences, using two or three intrinsic Ge detectors. In fig. 1 we display the X-ray spectra obtained in the Ge detector of highest resolution (0.5 keV FWHM), for 94.5 MeV  ${}^6\text{Li} + {}^{194}\text{Pt}$ ,  ${}^{197}\text{Au}$ . The singles spectra at the top of fig.1

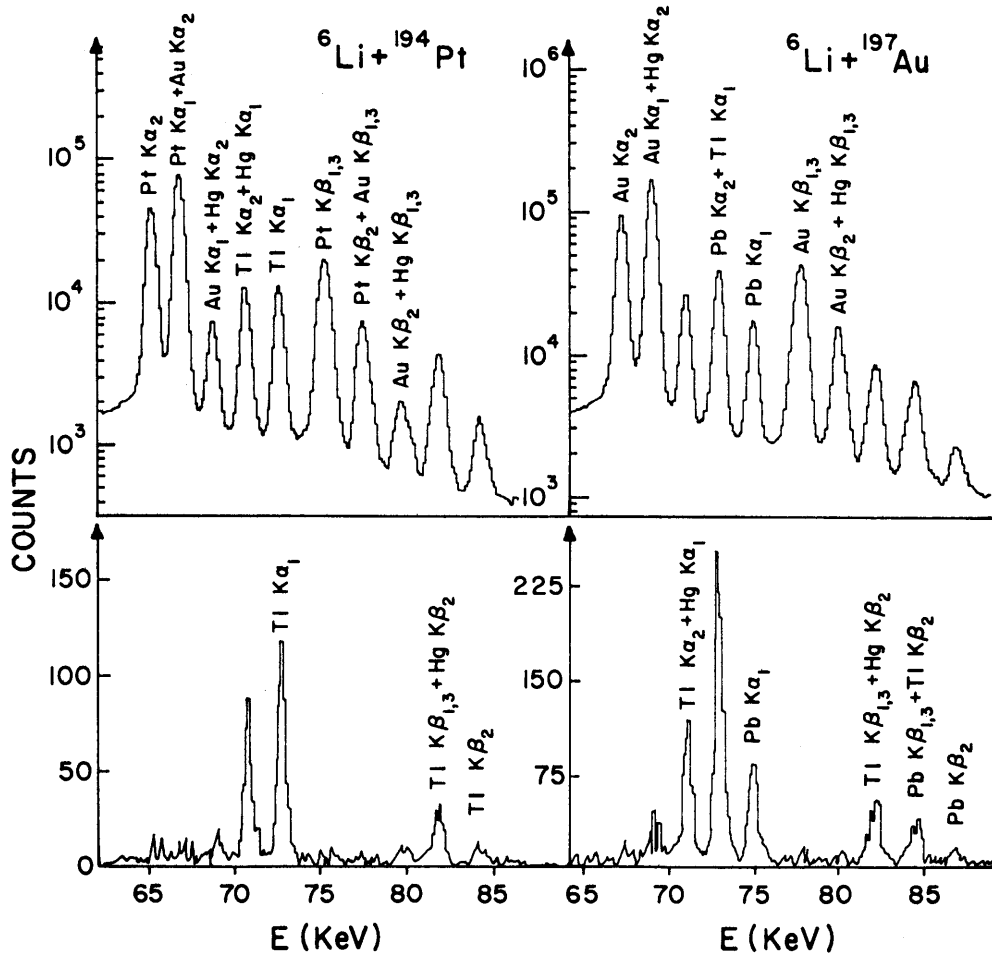


Figure 1. Representative singles (above) and coincidence (below) spectra for K X-rays. The bottom spectra were obtained in prompt coincidence (resolving time  $\approx 150$  nsec) with a K X-ray in a second Ge detector. The ratio of coincidence to singles events in the compound-nucleus ( $Z + 3$ )  $\text{Ka}_1$  peak is used in determining  $\langle M_K \rangle$ .

exhibit  $K\alpha_1$ ,  $K\alpha_2$ ,  $K\beta_1$  and  $K\beta_2$  X-ray lines characteristic of the elements from the target (Z) to the compound nucleus (Z+3). Many of these peaks are overlapping (the separation between  $K\alpha_1$  and  $K\alpha_2$  in each element is almost identical to the spacing of  $K\alpha_1$  lines from successive elements). However, the  $K\alpha_1$  peak from Z+3 (Tl for the Pt target, Pb for the Au target) is cleanly separated from all others and, unlike the others, has no contribution from  $\beta$ -activity. The bottom spectra in fig.1 are obtained in prompt coincidence with a K X-ray in the second Ge detector, which has lower energy resolution ( $\sim 2.0$  keV FWHM). The subtraction of backgrounds arising from accidental coincidences, and from coincidences between an X-ray in one detector and a Compton scattered  $\gamma$ -ray in the other, has essentially completely removed the target X-ray peaks from the coincidence spectra.

The singles yield of (Z+3) K X-rays in detector 1, with X-ray efficiency  $\eta_1$ , is

$$N_1(Z+3) \approx \sigma_{xn} \langle M_K \rangle \eta_1. \quad (1)$$

Here  $xn$  represents the total ( ${}^6\text{Li}, xn$ ) cross section, summed over all values of  $x$ , and the multiplicity is an appropriate weighted average over all  $\gamma$ -decay paths in all ( ${}^6\text{Li}, xn$ ) products. The singles yield should be isotropic to very good approximation, and measurement at a single angle allows determination of the absolute cross section  $\sigma_{xn}$  if  $\langle M_K \rangle$  can be determined. Comparison of the singles yield with the number  $N_{12}$  of coincidences between Z+3 K X-rays in detectors 1 and 2 (efficiency  $\eta_2$ ) gives:

$$\frac{N_{12}(Z+3)}{N_1(Z+3) \cdot \eta_2} = \frac{\langle M_K(M_K-1) \rangle}{\langle M_K \rangle} = \frac{\langle M_K^2 \rangle - 1}{\langle M_K \rangle} \quad (2)$$

$$\langle M_K \rangle + \frac{\Delta_K^2}{\langle M_K \rangle} - 1.$$

In the latter expression  $\Delta_K^2$  represents the variance of the K X-ray multiplicity distribution averaged over all  $xn$  products. Unlike the situation for  $\gamma$ -ray

multiplicities, where the shape of the multiplicity distribution must closely reflect the spin distribution in the de-exciting residue, the X-ray distribution must be more statistical in nature since internal conversion is a completely random event. We have assumed so far a Poisson multiplicity distribution, for which  $\Delta_K^2 = \langle M_K \rangle$ , and hence the coincidence/singles ratio yields  $\langle M_K \rangle$  directly.

It is expected that the values of  $\langle M_K \rangle$  extracted under the above assumption will not be in error by more than  $\pm 10\%$  (for  $\langle M_K \rangle \geq 2$ ), since the sharper multiplicity distributions characterizing any one decay path in any one  $xn$  product must be somewhat broadened when averaged over the various decay paths and various products contributing to the observed multiplicity. This expectation appears to be confirmed by our recent measurements of K X-ray- $\gamma$ -ray coincidence yields, using a Ge(Li) detector in addition to three intrinsic Ge X-ray detectors (see fig. 2). Comparison of coincidence and singles yields for specific  $\gamma$ -ray lines directly determines the value of  $\langle M_K \rangle$  characterizing the de-excitation of specific nucleides. Analysis of the data for 85 MeV  ${}^6\text{Li} + {}^{197}\text{Au}$ , leading to dominant  $xn$  products  ${}^{195,196,197}\text{Pb}$ ,

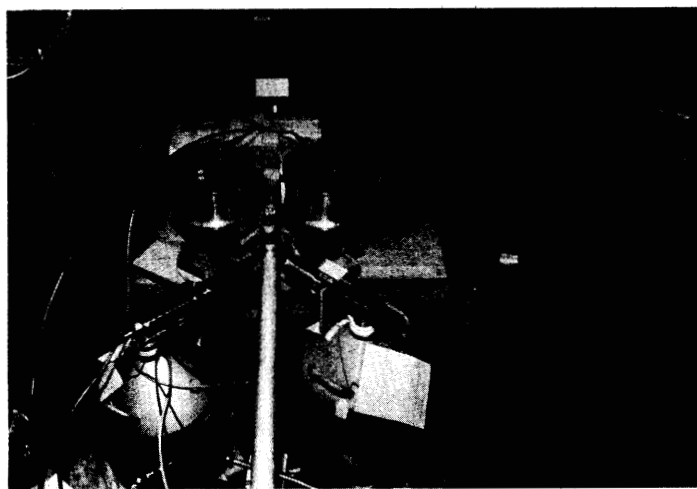


Figure 2. Setup for simultaneous measurement of X-ray-X-ray and X-ray- $\gamma$ -ray coincidence yields. Three intrinsic Ge detectors (at  $\pm 45^\circ$ ,  $135^\circ$ ) and one Ge(Li) detector ( $-135^\circ$ ) surround the target, mounted in a thin-walled (0.032") Al chamber. The plastic scintillator near the top serves as a monitor to trigger pulsers for dead-time correction.

Table I

Measured K X-ray Multiplicities ( $\langle M_K \rangle$ ) and Total ( ${}^6\text{Li}, xn$ ) Cross Sections ( $\sigma_{xn}$ )<sup>a)</sup>

Target	$E_{\text{lab}}=74.8 \text{ MeV}$		$E_{\text{lab}}=84.9 \text{ MeV}$		$E_{\text{lab}}=94.5 \text{ MeV}$	
	$\langle M_K \rangle$	$\frac{\sigma_{xn}}{\text{(mb)}}$	$\langle M_K \rangle$	$\frac{\sigma_{xn}}{\text{(mb)}}$	$\langle M_K \rangle$	$\frac{\sigma_{xn}}{\text{(mb)}}$
181Ta	1.24	827			1.22	720
194Pt			3.06	847	3.40	623
198Pt	2.99	942	3.24	921	3.41	746
197Au	2.10	651	2.50	566	2.08	556
208Pb	2.16	768	1.84	793	2.70	573

a) The relative measurement uncertainties for all results in this table are  $\pm 5 - 10\%$ . In addition there are absolute normalization uncertainties of  $\sim \pm 10\%$ , arising from absolute efficiency calibrations in the case of  $\langle M_K \rangle$  and from target-thickness measurements and beam integration for  $\sigma_{xn}$ , and possible systematic errors of  $\sim \pm 10\%$  arising from deviations from a Poisson X-ray multiplicity distribution.

and for  $85 \text{ MeV } {}^6\text{Li} + {}^{198}\text{Pt} \rightarrow {}^{195,196,197}\text{Tl}$ , reveals average values of  $\langle M_K \rangle$  consistent, within experimental uncertainties ( $\pm 10-15\%$ ), with the value determined from X-ray-X-ray coincidences, and surprisingly little change in  $\langle M_K \rangle$  between neighboring isotopes.

In Table I we summarize the values of  $\langle M_K \rangle$  obtained from eq. (2) (assuming  $\Delta_K^2 = \langle M_K \rangle$ ) and the values of  $\sigma_{xn}$  obtained from eq. (1) for the targets and energies studied so far.  $\langle M_K \rangle$  is higher, by factors of 1.5-2, for Tl compound nuclei than for the others studied. This feature is also reflected dramatically by the change in the relative intensities of Z+2 and Z+3 K X-rays between the two coincidence spectra shown in fig. 1. On the other hand, the relatively smooth energy dependence of  $\langle M_K \rangle$  for a given target, and the similar results for  ${}^{194}\text{Pt}$  and  ${}^{198}\text{Pt}$ , appear to confirm the absence of strong sensitivity to neutron number in the dominant xn residues.

Absolute normalization of the X-ray yields has been obtained from Faraday-cup beam integration, target thicknesses measured via Rutherford scattering, and radioactive-source efficiency calibrations (in determining  $\sigma_{xn}$ , only the efficiency ratio  $\eta_2/\eta_1$  is needed). With this method of normalization, we find interesting anomalies in target X-ray production cross sections, which are being further investigated. We

plan to further check the validity of our technique for measuring  $\sigma_{xn}$  by alternative measurements of in-beam  $\gamma$  singles or off-line activities for a few of the cases included in Table I; it is difficult, however, to reduce measurement uncertainties in these alternative techniques to the level easily attainable in the X-ray-X-ray method.

Experimental constraints on the origin of the relatively large number ( $\approx 2-3$ ) of K X-rays observed are imposed by 1) the known low-lying yrast transitions in many of the populated xn residues, 2) the X-ray- $\gamma$ -ray coincidence data, and 3) our measured total fusion cross sections  $\sigma_{fus}$  (see next contribution). Only a very small fraction of the observed X-rays from Pb isotopes can be attributed to internal conversion of known yrast transitions from states with  $J \lesssim 12$ . Extensive X-ray side-feeding of these low-lying states is ruled out by the near-constancy of  $\langle M_K \rangle$  deduced from coincidences with the various known  $\gamma$ -lines. Furthermore, coincidences between delayed  $\gamma$ 's depopulating the  $12^+$  0.27  $\mu\text{sec}$  isomer in  ${}^{196}\text{Pb}$  (see ref. 3) and prompt X-rays (see fig. 3) show that nearly all of the  ${}^{196}\text{Pb}$  K X-rays feed the  $12^+$  state. On the other hand, the relatively small  $\sigma_{fus}$  for these systems limits the average spin at which the residues are populated to  $\langle J \rangle \approx 16-20$ , unless we assume that there is a lower

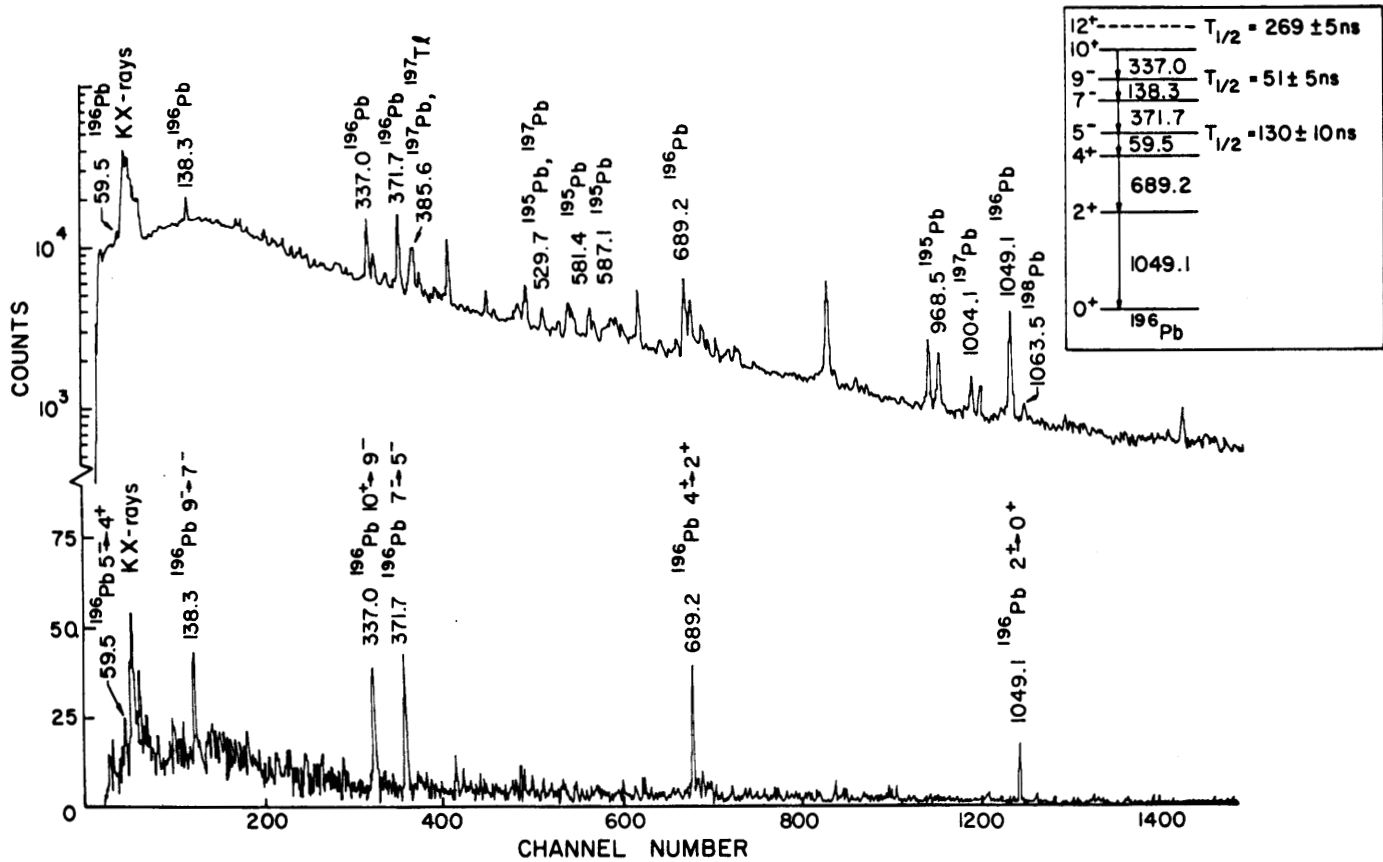


Figure 3. Top: singles Ge(Li) spectrum obtained for 85 MeV <sup>6</sup>Li + <sup>197</sup>Au. Only identified lines in the (<sup>6</sup>Li,αn) products are labeled. Bottom: spectrum of Ge(Li) events delayed (by 215 - 450 nsec) with respect to a (Z + 3) K<sub>α1</sub> X-ray. The transitions depopulating the 12<sup>+</sup> isomer in <sup>196</sup>Pb show up prominently. Insert: level scheme for the known yrast states in <sup>196</sup>Pb, from ref. 3. Analysis of the coincidence/singles ratio for the 337-keV transition indicates that 2.3 ± 0.2 K X-rays arise from above the 12<sup>+</sup> isomer.

angular-momentum cutoff on fusion reactions. The dominant contribution to  $\langle M_K \rangle$  in the Pb isotopes thus appears to arise from a small region of spin values. Since the number of K X-rays emitted per E2 transition (for Z = 82) is  $\lesssim 0.14$  for all transition energies (= 0.14 for  $E_\gamma = 150$  keV), this suggests a preponderance of relatively low-energy M1 transitions among the yrast and/or pre-yrast states in this mass and spin region. This feature would be consistent with mildly deformed oblate nuclear shapes.<sup>4</sup>

We are presently planning other experiments to further constrain the origin of the X-rays and to examine the systematic behavior of  $\langle M_K \rangle$  over a wider region of bombarding energy and targets.

\*Ohio State University, Columbus, Ohio

1. G. Deconninck and N. Longequeue, Phys. Rev. Lett. 30, 863 (1973).
2. G. Deconninck and M. Longr e, Phys. Rev. A16, 1390 (1977).
3. C. Roulet, et al., Nucl. Phys. A285, 156 (1977).
4. L.K. Peker, J.H. Hamilton, and J.O. Rasmussen, Phys. Rev. Lett. 41, 457 (1978).